Cell Host & Microbe
Article

The DNA Damage-Regulated Autophagy Modulator DRAM1 Links Mycobacterial Recognition via TLR-MYD88 to Autophagic Defense

Michiel van der Vaart,[1] Cornelis J. Korbee,[2] Gerda E.M. Lamers,[1] Anouk C. Tengeler,[1] Rohola Hosseini,[1] Mariëlle C. Haks,[2] Tom H.M. Ottenhoff,[2] Herman P. Spaink,[1] and Annemarie H. Meijer[1,*]
[1]Institute of Biology, Leiden University, 2333 CC Leiden, the Netherlands
[2]Department of Infectious Diseases, Leiden University Medical Center, 2300 RC Leiden, the Netherlands
*Correspondence: a.h.meijer@biology.leidenuniv.nl
http://dx.doi.org/10.1016/j.chom.2014.05.005

SUMMARY

Autophagy is an important defense mechanism against mycobacteria, the causative agents of tuberculosis. The molecular mechanisms that link mycobacterial recognition to autophagy remain unclear. Our analysis in zebrafish and human macrophage models of mycobacterial infection reveals that the DNA damage-regulated autophagy modulator DRAM1 functions downstream of pathogen recognition by the Toll-like receptor (TLR)/interleukin-1 receptor (IL1R)-MYD88-NF-κB innate immune sensing pathway to activate selective autophagy. Mycobacterial infection of human macrophages and zebrafish embryos induced *DRAM1* expression in a MYD88 and NF-κB-dependent manner. DRAM1 knockdown increased mycobacterial infection, whereas overexpression lowered infection by hyperactivating autophagy. DRAM1-mediated selective autophagic defenses require the cytosolic DNA sensor STING and the selective autophagy receptor p62/SQSTM1. Contrary to its known role in autophagy-mediated cell death and cancer, this DRAM1 function is p53 independent. We propose that DRAM1 mediates autophagic defense against a broader range of intracellular pathogens, since *DRAM1* expression was also induced by the common bacterial endotoxin lipopolysaccharide.

INTRODUCTION

A growing body of evidence firmly establishes autophagy as a defense mechanism against intracellular pathogens (Deretic et al., 2013). Autophagy is an evolutionary conserved process in eukaryotes essential for cellular homeostasis in response to environmental and cellular stressors. During autophagy (or macroautophagy), cytoplasmic components are enveloped in double-membraned autophagosomes that fuse with lysosomes for degradation of their content in a process known as autophagic flux. Selective autophagy specifically degrades unwanted protein aggregates or cellular contents via ubiquitin-mediated targeting, using receptors such as p62/SQSTM1 and NDP52 to link ubiquitinated cargo to the microtubule-associated protein 1 light chain 3 (LC3) (Deretic et al., 2013). Subsequently, components of the general autophagy machinery, including the ATG12-ATG5-ATG16L1 complex, are required for autophagosome maturation (Levine et al., 2011). Autophagy has diverse roles in defense by contributing to cytokine secretion, targeting microbes for lysosomal degradation, and as regulator of innate and adaptive immune responses (Levine et al., 2011; Deretic et al., 2013).

Studies on *Mycobacterium tuberculosis* (*Mtb*), the causative agent of pulmonary tuberculosis (TB), have been a leading example of how autophagy can counteract the ability of intracellular pathogens to avoid host defenses (Alonso et al., 2007; Gutierrez et al., 2004; Singh et al., 2006; Deretic et al., 2013). Mycobacteria evade leukocyte bacterial-killing mechanisms by preventing phagosome-lysosome fusion, creating a niche that allows them to survive and proliferate (Vergne et al., 2004). Infected macrophages then recruit other immune cells to form highly organized structures known as granulomas (Ramakrishnan, 2012).

We used the zebrafish model to study the role of autophagy during early stages of mycobacterial infection. *Mycobacterium marinum* (*Mm*) is a natural fish pathogen and a close relative of *Mtb*. It causes a phenotype in zebrafish that highly resembles human TB disease, including the formation of caseating granulomas (Swaim et al., 2006). *Mm* infection of zebrafish embryos has been successfully used to understand host cell signaling and mycobacterial virulence determinants during TB disease (Berg and Ramakrishnan, 2012). The zebrafish model allows visualization of host-pathogen interactions during early stages of mycobacterial pathogenesis in the absence of an adaptive immune contribution (Clay et al., 2007) and has recently been used as an in vivo model to study bacterial autophagy (Mostowy et al., 2013).

The molecular signaling pathway responsible for autophagic control of mycobacterial disease remains unclear, although there are strong links between pathogen recognition by Toll-like receptors (TLRs) and autophagy induction (Delgado et al., 2008; Ponpuak et al., 2010; Sanjuan et al., 2007; Shi and Kehrl, 2008). We employed our myeloid differentiation primary response 88 (*myd88*) mutant zebrafish line to study regulation of autophagy downstream of this central Toll-like receptor

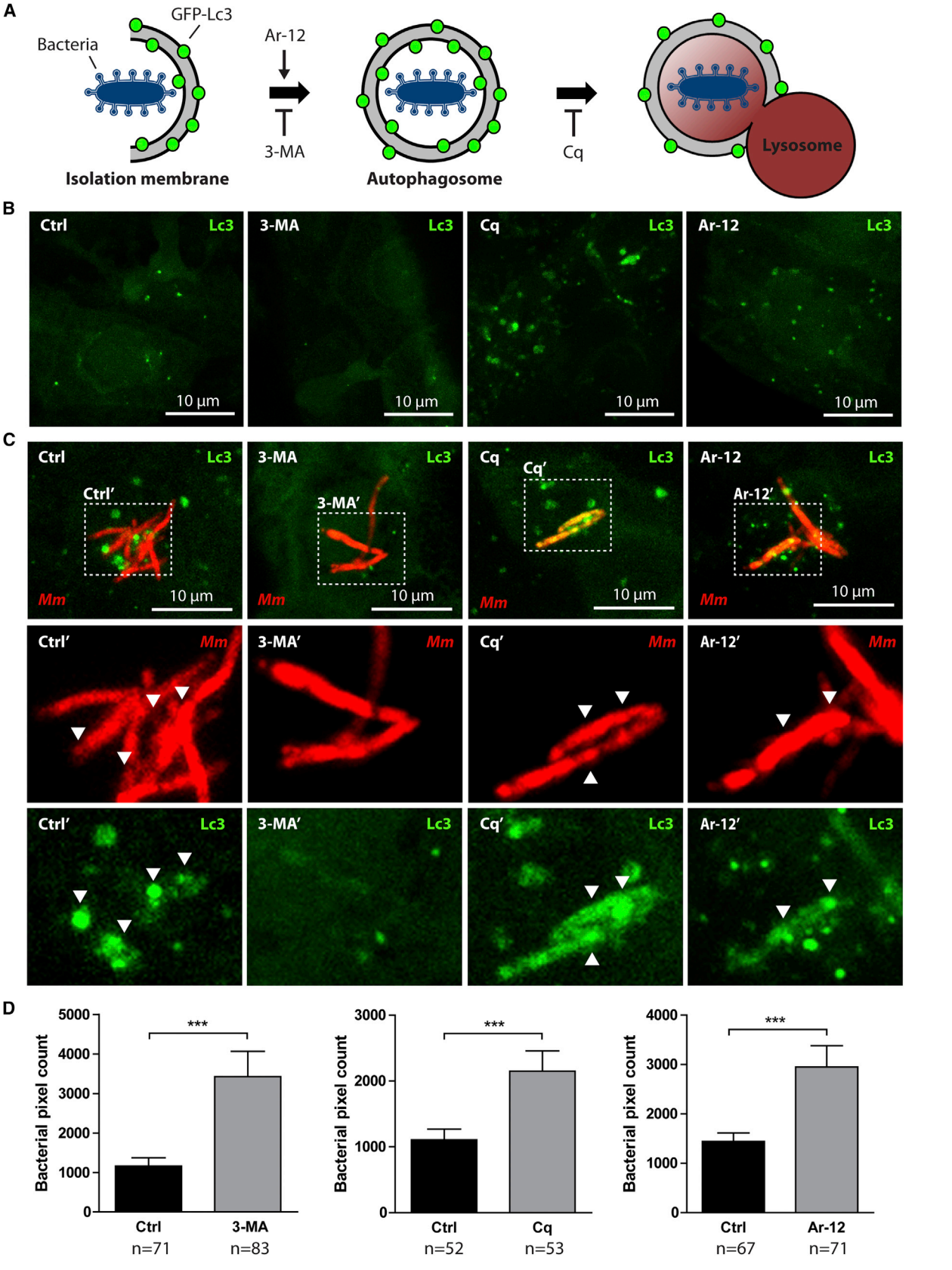

(legend on next page)

(TLR)/interleukin-1 receptor (IL1R)-signaling adaptor (van der Vaart et al., 2013). We found that DNA damage-regulated autophagy modulator 1 (*dram1*) expression during mycobacterial infection requires MyD88. *DRAM1* is a known target gene of the tumor suppressor p53 and is required for p53-dependent cell death by inducing autophagy (Crighton et al., 2006). There is considerable interest in DRAM1 due to its relation with tumor development and cancer therapy (Galavotti et al., 2013; Ryan, 2011).

Here, we show that *DRAM1*/*dram1* expression during mycobacterial infection in primary human macrophages and zebrafish embryos depends on the TLR/IL1R-MYD88-NF-κB signaling pathway central to innate immunity and does not require p53. DRAM1 colocalizes with intracellular mycobacteria, and knockdown results in higher bacterial burdens. Confocal imaging, supported by electron microscopy (EM), showed that Dram1 is needed for the formation of autophagosomes and promotes lysosome formation and autophagic flux. Furthermore, we show that the function of *dram1* requires the selective autophagy receptor p62 and the STING DNA-sensing pathway and that activation of this selective autophagy pathway by overexpressing *dram1* in zebrafish embryos is protective against TB disease.

RESULTS

Activating General Autophagy Is Not Beneficial for In Vivo Defense against Mycobacteria

To investigate autophagic defense in zebrafish, we first tested widely used autophagy modulators in GFP-Lc3 transgenic embryos (He et al., 2009). This confirmed that 3-methyladenine (3-MA) inhibits autophagosome formation, while chloroquine (Cq) and Ar-12 increased the number of Lc3 fluorescent punctae (Figures 1A and 1B). The effect of Cq treatment is consistent with its prohibitive action on autophagic flux by preventing autophagosome-lysosome fusion, resulting in accumulation of Lc3-labeled autophagosomes. Ar-12 inhibits PDK1/AKT signaling, causing accumulation of reactive oxygen species (ROS) and triggering a stress-induced autophagic response (Gao et al., 2008). We then infected GFP-Lc3 embryos with *Mm* and treated them with 3-MA, Cq, or Ar-12 for the first 24 hr postinfection (hpi). Colocalization with GFP-Lc3 was observed for ~30% of the bacteria in control embryos, consistent with results in cultured macrophages (Lerena and Colombo, 2011). 3-MA decreased autophagy induction in infected cells (Figure 1C). Blocking autophagic flux with Cq led to an accumulation of autophagosomes colocalized with *Mm* (Figure 1C). In this example, Cq treatment prevented the maturation of bacterial compartments that were entirely decorated with Lc3. Ar-12-treated embryos showed many small Lc3 punctae throughout infected cells, mostly not associated with bacteria (Figure 1C). Next, we quantified the effect of these drugs on the bacterial burden at 3 days postinfection (3 dpi) and observed increased infection after treatment with all compounds (Figure 1D). The effects of inhibitors, 3-MA and Cq, are consistent with results in mammalian cell cultures infected with mycobacteria (Gutierrez et al., 2004) and support autophagy to function in defense against mycobacteria in zebrafish. However, stimulating ROS-inducible nontargeted autophagy by Ar-12 or the starvation-induced mammalian target of rapamycin (mTOR) pathway using rapamycin (Figure S1, available online) was also detrimental to defense against mycobacteria in our zebrafish model.

Induction of Autophagy Modulator *dram1* by Mycobacterial Infection Is MyD88 Dependent in Zebrafish

It remains largely unknown how TLR pathogen recognition and autophagy are connected. We have previously demonstrated that *myd88* mutant (*myd88*$^{-/-}$) zebrafish embryos, lacking a signaling adaptor vital to TLR signaling, show impaired induction of genes central to innate immunity and are more susceptible to infection by *Mm* (van der Vaart et al., 2013). Microarray profiling of *myd88*$^{+/+}$ and *myd88*$^{-/-}$ embryos infected with *Mm* confirmed the significantly lower expression of proinflammatory genes, such as *il1b*, *tnfa*, and *mmp9*, in the absence of MyD88 signaling (Figure 2A). In our search for regulators linking pathogen recognition to autophagy, we found that expression of *dram1* was significantly reduced during *Mm* infection in the absence of functional MyD88 (Figure 2A). This gene encodes a transmembrane protein that is highly conserved among vertebrates in terms of protein homology and gene synteny (Crighton et al., 2006) (Figures S2A–2C). Over a time course of *Mm* infection, *dram1* expression progressively increased in infected *myd88*$^{+/+}$, but not in *myd88*$^{-/-}$ (Figure 2B). The MyD88 dependency of *dram1* during *Mm* infection was confirmed by RNA sequencing and quantitative PCR (qPCR) in independent experiments (Figures 2A and 2C). Increased expression of the genes encoding p53, Atg5, Lc3, or p62 was not detected on the whole-embryo level.

In silico analysis of the promoter regions of human and zebrafish *DRAM1*/*dram1* revealed conserved binding sites for the hematopoietic transcription factor Pu.1 (Figure S2D). Expression of *dram1* in leukocytes was confirmed by qPCR on fluorescence-activated cell sorted (FACS) immune cell populations, showing its enrichment in the Mpeg1^{+} (Ellett et al., 2011), Mpx^{+} (Renshaw et al., 2006), and Lck^{+} (Langenau et al., 2004) fractions of dissociated transgenic embryos specific for macrophages, neutrophils, and lymphocytes, respectively (Figure 2D). We conclude that zebrafish *dram1* is expressed in myeloid and lymphoid immune cell lineages and induced in a MyD88-dependent fashion following infection by mycobacteria.

Figure 1. Stress-Induced Autophagy Is Not Beneficial for Defense of Zebrafish Embryos against Mycobacterial Infection

(A) Schematic representation of the effects of 3-MA, Cq, and Ar-12 on autophagosome formation and autophagic flux.

(B) GFP-Lc3 embryos 2 dpf were treated for 24 hr with DMSO (control), 3-MA, Cq, or Ar-12. Representative confocal micrographs of endothelial cells at 3 dpf are shown.

(C) GFP-Lc3 embryos treated as described for (A) injected with *Mm*. Representative confocal micrographs of infected cells at 3 dpf are shown. Boxed areas are detailed below; arrowheads indicate overlap between *Mm* and Lc3.

(D) AB/Tupfel long fin (AB/TL) embryos treated as described for (A) infected with *Mm*. Bacterial pixel counts were determined at 3 dpi.

Data (mean ± SEM) is pooled from at least two individual experiments ($n \geq 50$ embryos per group). See also Figure S1.

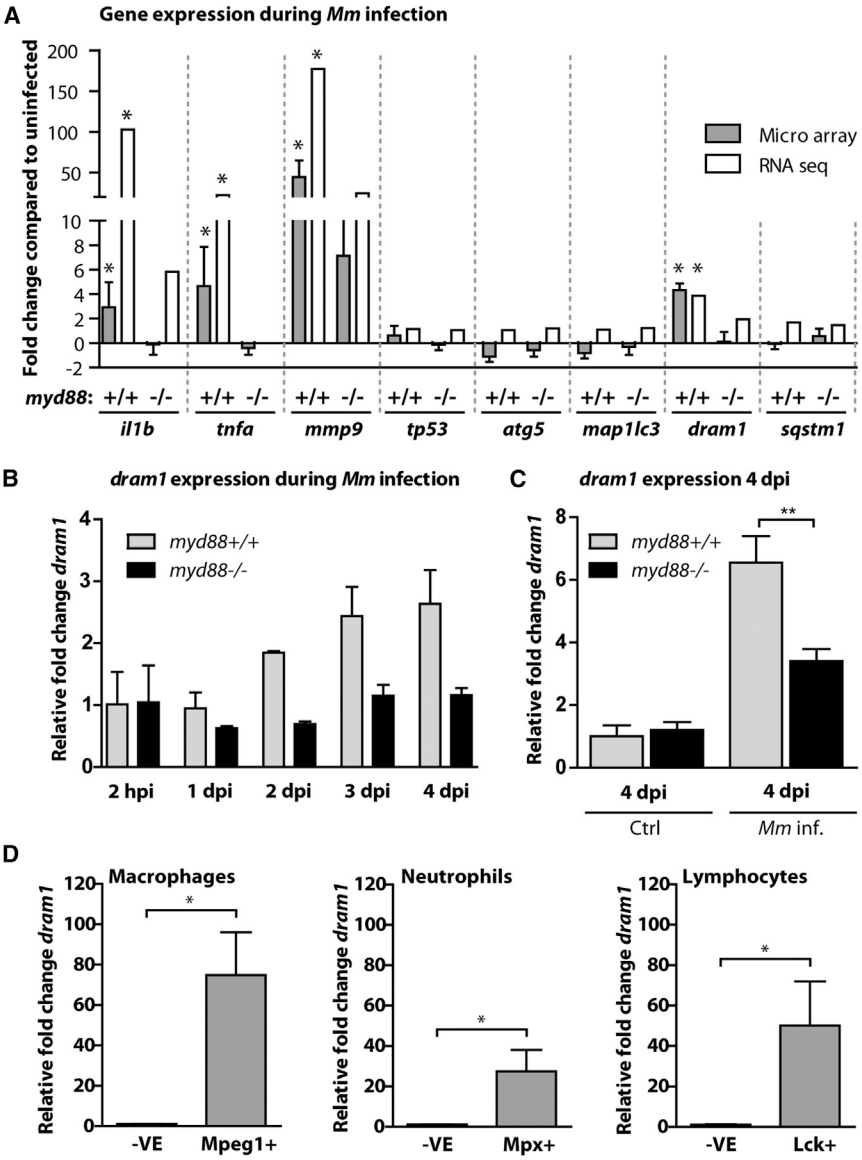

Figure 2. *dram1* Is Induced by Mycobacterial Infection in a Myd88-Dependent Fashion

(A) *myd88*$^{+/+}$ and *myd88*$^{-/-}$ embryos infected with *Mm* were snap frozen individually at 4 dpi, and triplicate samples were compared with PBS-injected controls using a common reference microarray design. Observed differences were confirmed by RNA sequencing of pools (n = 20 embryos) of uninfected and *Mm*-infected *myd88*$^{+/+}$ and *myd88*$^{-/-}$ embryos.

(B) Expression of *dram1* at multiple time points after infection was analyzed by qPCR on pools of *Mm*-infected *myd88*$^{+/+}$ and *myd88*$^{-/-}$ embryos, relative to PBS-injected controls (mean ± SEM of n = 2 biological replicates with 20 embryos per pool).

(C) Expression levels of *dram1* at 4 dpi in individual *myd88*$^{+/+}$ and *myd88*$^{-/-}$ embryos with or without infection were determined by qPCR (mean ± SEM of n = 3 biological replicates with 10 embryos per pool).

(D) Macrophages, neutrophils, and leukocytes from 5–6 dpf larvae were isolated by FACS. Expression of *dram1* in the positive fractions (e.g., Mpeg1^{+}) relative to the negative fractions (−VE) was determined by qPCR (mean ± SEM of n = 4 biological replicates). See also Figure S2.

tion factor downstream of MyD88 regulating *dram1* expression during mycobacterial infection. Since the application of a previously described NF-κB activation inhibitor (NAI) for the duration of early *Mm* pathogenesis (2–4 dpi) was harmful to embryonic development (Kanther et al., 2011), we developed an alternative assay to test for the involvement of NF-κB activity based on two previous findings: (1) zebrafish *dram1* expression is induced by *Salmonella enterica* serovar Typhimurium (*St*) infection (Stockhammer et al., 2010) and (2) TLR recognition of *St*-derived lipopolysaccharide (LPS) in zebrafish depends on MyD88 (van der Vaart et al., 2013). Since LPS-induced gene expression occurs rapidly after exposure, this allowed us to avoid harmful effects of NAI treatment by blocking NF-κB activity for only 4 hr. We found that LPS exposure significantly increased *dram1* expression in control-treated embryos, which was completely abrogated by NAI (Figure 3C). Furthermore, *myd88*$^{-/-}$ embryos did not increase *dram1* expression in response to LPS, while *p53*$^{-/-}$ embryos behaved identical to wild-type controls (Figure 3C). Expression levels of the known NF-κB target gene serum amyloid A (*saa*) displayed a similar pattern following LPS exposure (Figure 3D). Together, these data demonstrate that bacterial induced expression of *dram1* is dependent on MyD88-NF-κB, but not on p53.

Bacterial-Induced Expression of *dram1* Is Independent of p53 but Dependent on NF-κB

Since the known functions of DRAM1 are dependent on p53 signaling, we analyzed expression of *dram1* in embryos with a mutation in the DNA-binding domain of p53 (*p53*$^{-/-}$) (Guo et al., 2013). *Mm*-infected *p53*$^{-/-}$ mutants showed upregulation of *dram1* to wild-type levels, indicating that infection-induced *dram1* expression is p53 independent (Figure 3A). As a control, we treated embryos with the p53-stabilizing agent roscovitin (Guo et al., 2013). Unlike wild-type, *p53*$^{-/-}$ embryos were insensitive to roscovitin-induced malformations and did not express *dram1* upon treatment (Figures S3, 3B). These results show that the canonical p53-dependent route to *dram1* induction is functional in zebrafish but not employed during *Mm* infection. Autophagy can be regulated by NF-κB activation (Criollo et al., 2010), and the promoter regions of human and zebrafish *dram1* contain predicted NF-κB consensus binding sites (Figure S2D). We hypothesized that NF-κB is the essential transcrip-

DRAM1 Is under Control of NF-κB and Colocalizes with *Mtb* in Human Macrophages

In view of the strong evolutionary conservation of DRAM1, we hypothesized that the signaling pathway controlling *dram1*

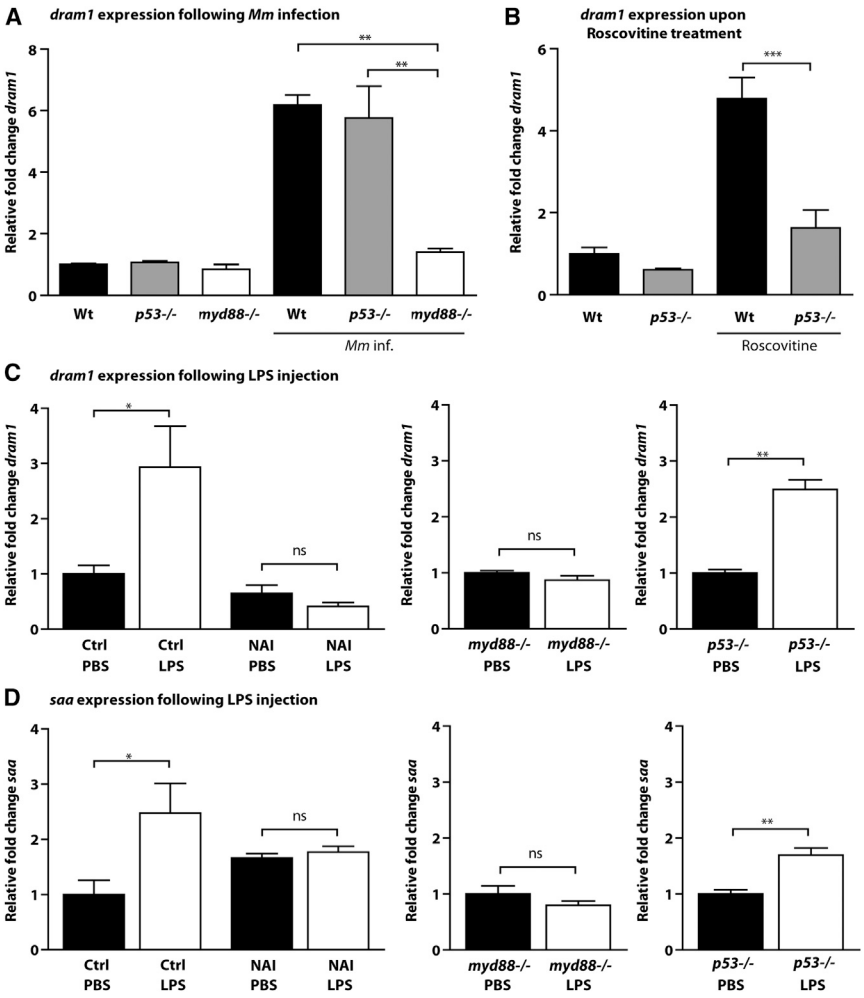

Figure 3. *dram1* Expression during Mycobacterial Infection Is Independent of p53 but Dependent on NF-κB

(A–C) Expression levels of *dram1* were determined by qPCR for (A) wild-type, *p53*$^{-/-}$, and *myd88*$^{-/-}$ embryos 4 days after infection with *Mm*, relative to mock-injected controls; (B) wild-type and *p53*$^{-/-}$ embryos at 5 dpf after 24 hr of treatment with roscovitine, relative to untreated controls (see also Figure S3); and (C) 1 dpf embryos at 2 hpi with LPS, relative to their respective PBS-injected controls (left panel: wild-type embryos with or without NAI treatment [4 hr total, including 2 hr pretreatment]; middle panel: *myd88*$^{-/-}$ embryos; right panel: *p53*$^{-/-}$ embryos).

(D) Expression levels of *saa* were determined by qPCR under the same conditions as those described for (C).

All graphs show data (mean ± SEM) from three biological replicates with n = 20 embryos pooled per replicate. See also Figures S2 and S3.

during mycobacterial infection is conserved between human and zebrafish. We obtained human primary macrophages type 1 (M1) and type 2 (M2) from peripheral blood mononuclear cells and infected them with *Mtb*. At 4 hpi we detected elevated expression levels of *DRAM1* in infected M1 and M2 (Figure 4A). In addition, *SQSTM1* (p62) was significantly induced in *Mtb*-infected M1 and M2 macrophages (Figure 4B), suggesting a collaboration between the autophagy-related proteins DRAM1 and p62 during mycobacterial infection. *IL1β* expression was also induced in these macrophages, confirming the inflammatory response to infection (Figure 4C). Treatment with NAI prevented the expression of *DRAM1* in infected M1 and M2 (Figure 4A), while SQSTM1 and IL1β were partially dependent on NF-κB activity in M1 and independent of NF-κB in M2 macrophages (Figures 4B and 4C). Using siRNA depletion of MYD88, we could confirm the conservation of the MYD88-NF-κB-DRAM1 signaling route during *Mtb* infection of human M2, but not M1 (Figure 4D), indicating further complexity in DRAM1 regulation in differentiated human macrophages. In both M1 and M2 macrophages we observed clear colocalization of DRAM1 and LC3 with Mtb at 72 hpi (Figures 4E and 4F). siRNA against *DRAM1*, while effectively reducing *DRAM1* mRNA levels, unexpectedly did not lead to reduced protein expression (Figure S4). As the stability of DRAM1 protein therefore precludes the use of genetic knockdown as an experimental approach to study the impact of DRAM1 on mycobacterial infection in human cells, we performed further functional studies in the zebrafish in vivo model.

Dram1 Is Required to Contain Mycobacterial Growth inside Macrophages

To investigate the hypothesis that Dram1 functions in autophagic defense against mycobacterial infection, we used an antisense morpholino oligonucleotide approach in zebrafish to block intron-exon splicing (Figure S5), thus preventing the production of functional Dram1 protein. Dram1 deficiency caused by two unique morpholino sequences significantly increased *Mm* bacterial burdens (Figure 5A). It was previously shown in glioblastoma stem cells that DRAM1 is required for localization of p62 to autophagosomes, suggesting a role for DRAM1 in p62-dependent selective autophagy (Galavotti et al., 2013). *Mtb* can permeabilize the phagosomal membrane using virulence factors encoded by the bacterial region of difference 1 (RD1), allowing cytosolic components of the selective autophagy pathway access to bacteria inside these vacuoles (Watson et al., 2012). Recognition of extracellular bacterial DNA by the STING DNA-sensing pathway leads to degradation of ubiquitinated *Mtb* in mature autophagolysosomes via p62 (Watson et al., 2012). We therefore depleted the zebrafish homologs of p62 and STING using morpholinos and found that this significantly increased mycobacterial burdens (Figures 5A and S5).

Interestingly, highly infected embryos with abrogated *dram1*, *sqstm1*, or *sting* expression displayed a similar phenotype with accumulation of bacteria inside intersegmental blood vessels, indicative of extracellular growth of bacteria (Figure 5B). In contrast, highly infected control embryos only displayed large

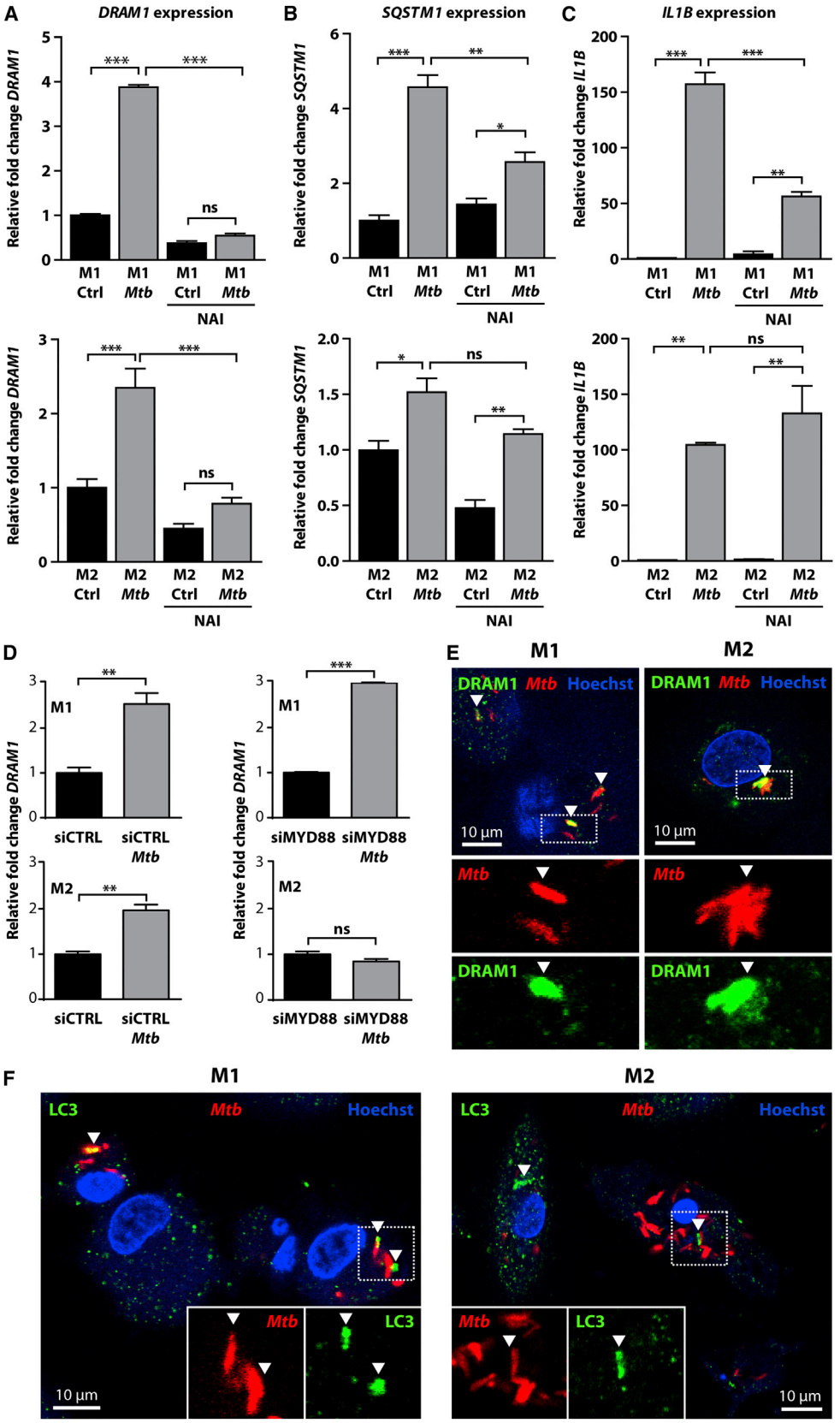

(legend on next page)

granuloma-like aggregates of *Mm*-infected cells. The phenotype of *dram1* knockdown embryos was not caused by a reduced number of neutrophils or macrophages (Figure 5C). Neither did *dram1* knockdown lead to decreased expression of the proinflammatory genes *il1b* and *mmp9*, ruling out the possibility that Dram1 is required for the initiation of inflammation. In contrast, Dram1-depleted embryos displayed significantly higher expression levels of *il1b* compared to control embryos with equal bacterial burdens at the time point of RNA isolation (Figures 5D and S5F).

Upon infection of zebrafish embryos, mycobacteria are rapidly phagocytosed by macrophages (Clay et al., 2007). We used a macrophage-specific reporter line with mCherry localized to all cellular membranes (Bernut et al., 2014) to study the intracellular localization of *Mm* upon knockdown of d*ram1*. In both the control and *dram1* knockdown group, virtually all *Mm* were phagocytosed at 1 dpi, and bacteria inside macrophages were enclosed by membranes (Figure S5G). At 2 dpi, bacteria remained intracellular and enclosed by membranes in control-infected embryos (Figure 5E). In contrast, we frequently found overgrown macrophages unable to contain *Mm* inside vesicles in the *dram1* knockdown group (Figure 5E), which coincided with the appearance of extracellular bacteria (Figure S5H). At 3 dpi, *Mm* in control-infected embryos were residing either in intracellular enclosures or freely in the cytoplasm, indicating that phagosomal escape eventually also occurred in wild-type embryos. However, this only occurred for *Mm* with a functional RD1 locus (Figure 5F), similar to the RD1-dependent phagosomal escape of *Mtb* in human cells (van der Wel et al., 2007). Using EM, we could confirm that most bacteria were contained inside phagosomes for control-infected embryos at 2 dpi (Figure 5G), with a small proportion of bacteria residing freely in the cytoplasm (Figure 5H). At the same time point, infected cells of Dram1-depleted embryos were overgrown by *Mm* and the vast majority of bacteria was cytoplasmic (Figure 5I). The inability of Dram1 morphants to control intracellular growth of mycobacteria frequently resulted in rupture of infected cells and the presence of extracellular bacteria inside blood vessels (Figures 5I and S5I).

Selective Autophagy Induced by *dram1* Overexpression Restricts Mycobacterial Infection

To further test the hypothesis that Dram1 is involved in autophagic defense against mycobacterial infection, we cloned zebrafish *dram1* and injected mRNA into GFP-Lc3 transgenic embryos at the one-cell stage, leading to ubiquitous overexpression of *dram1* in the developing embryo. Embryos overexpressing *dram1* developed normally and showed no apparent phenotypes (data not shown). At 3 days postfertilization (dpf), *dram1* overexpression resulted in significantly increased numbers of GFP-Lc3 vesicles compared to controls (Figures 6A and 6B), indicating that the function of DRAM1 as an inducer of autophagy is conserved between human and zebrafish (Crighton et al., 2006; Mah et al., 2012). Dram1 initiates GFP-Lc3 accumulation via a mechanism that is distinct from the autophagy response to Ar-12 or rapamycin treatment, since Dram1-depleted embryos still displayed a marked increase in GFP-Lc3 vesicles upon exposure to these drugs (Figures S6A and S6B). We then examined the effect of *dram1* overexpression during mycobacterial infection and observed that it reduced bacterial burden in a dose-dependent manner (Figures 6C and 6D). Mycobacterial clusters decreased in number and size in embryos injected with the highest dose of *dram1* RNA (Figures S6C and S6D), showing that Dram1 is part of a defense mechanism against mycobacterial infection. Both the induction of autophagy in *Mm*-infected cells and the increase in bacterial burden upon *dram1* knockdown required the mycobacterial RD1 virulence locus (Figures 6E and 6F). To further demonstrate the importance of Dram1 in defense against pathogenic mycobacteria, we knocked down the expression of *myd88* and *dram1* in GFP-Lc3 embryos and infected them with *Mm*. Morpholino knockdown of either *myd88* or *dram1* significantly reduced the number of GFP-Lc3 punctae per cell (Figures 6G and 6H). Strikingly, overexpression of *dram1* RNA increased the autophagy response in infected cells, showing a clear colocalization between Lc3 and bacteria, which occasionally completely encapsulated bacteria (Figures 6G and 6H). Morpholino knockdown of p62/*sqstm1* significantly lowered the number of GFP-Lc3 punctae per infected cell in zebrafish embryos (Figures 6G and 6I), consistent with previous observations in human cell cultures (Ponpuak et al., 2010; Watson et al., 2012). If autophagic defense initiated by Dram1 requires p62, Dram1-dependent autophagy should be blocked by depletion of p62. Indeed, coinjection of *sqstm1* morpholino with *dram1* RNA counteracted the increased formation of *Mm*-associated autophagosomes caused by *dram1* overexpression (Figures 6G and 6I). As was observed for p62, knockdown of *sting* also significantly lowered the number of GFP-Lc3 punctae per infected cell and could counteract the effect of *dram1* overexpression (Figures 6G and 6J). Together, these data demonstrate that Dram1 stimulates the targeting of autophagosomes to bacteria or bacteria-containing compartments, requiring Sting and the selective autophagy receptor p62. We conclude that this Dram1-mediated mechanism downstream of MyD88 has a protective function during mycobacterial infection in vivo.

Dram1 Mediates Autophagic Flux and Lysosomal Maturation via Multiple Vesicle Fusion Events

Autophagosomes require fusion with lysosomes to obtain mycobactericidal characteristics (Levine et al., 2011). It was previously reported that DRAM1 regulates autophagic flux through lysosomes following mitochondrial dysfunctioning (Zhang et al., 2013). We therefore used LysoTracker to examine the role of

Figure 4. DRAM1 Colocalizes with *Mtb* and Is Regulated by MYD88-NF-κB Signaling in Human Primary Macrophages

(A–C) The effect of NAI treatment on expression of (A) *DRAM1*, (B) *SQSTM1*, and (C) *IL1B* in M1 and M2 in the presence or absence of *Mtb* was determined by qPCR, relative to uninfected controls. All graphs show data (mean ± SEM) from three biological replicates.

(D) Expression of *DRAM1* in M1 and M2 transfected with siCTRL or siMYD88 with and without *Mtb* infection. All graphs show data (mean ± SEM) from three biological replicates.

(E and F) Immunohistochemistry for (E) DRAM1 (green) or (F) LC3 (green) performed on M1 and M2 at 72 hpi with *Mtb* (red); Hoechst staining (blue) was used to outline the nuclei and cell boundaries. See also Figure S4.

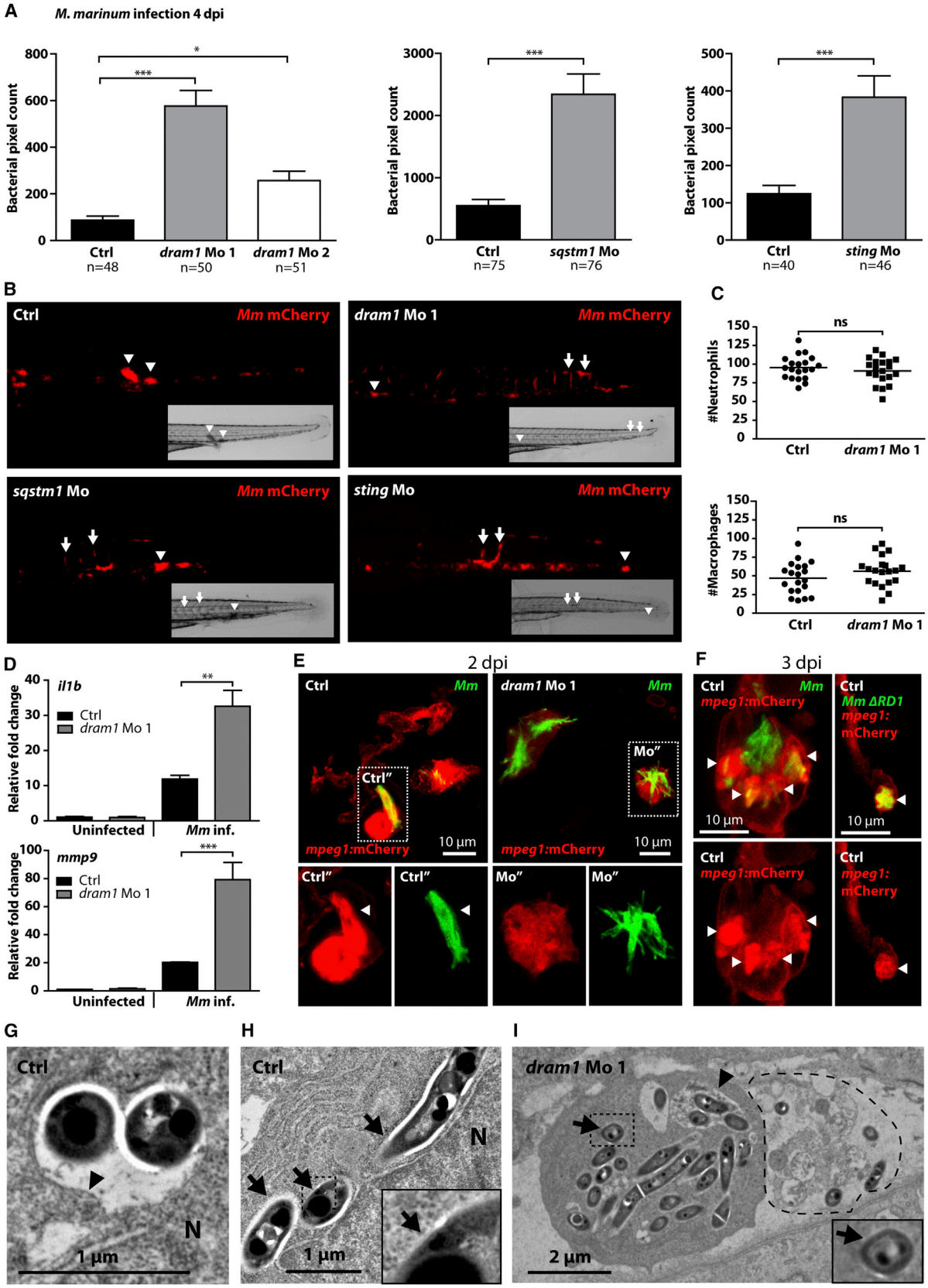

(legend on next page)

Dram1 in lysosomal acidification during *Mm* infection. Dram1 depletion abrogated colocalization of acidified lysosomes with *Mm*-containing vesicles, while Dram1 overexpression dramatically increased lysosomal acidification surrounding *Mm* (Figure 7A). Next, we demonstrated that autophagic flux contributes to this process by visualizing *Mm*-containing vesicles that are positive for LysoTracker as well as GFP-Lc3 (Figure 7B).

Human DRAM1 was described as a lysosomal protein with six predicted transmembrane domains and has also been localized to autophagosomes (Crighton et al., 2006; Mah et al., 2012). In agreement, zebrafish mCherry-Dram1 predominantly localized to LysoTracker-positive vesicles (Figure 7C). To express mCherry-Dram1, we injected a DNA construct with beta-actin promoter, resulting in transient mosaic expression and frequently showing high expression in muscle cells. Cells with high levels of mCherry-Dram1 contained large Dram1-positive vacuoles, while neighboring muscle cells retained their characteristic striated pattern (Figure 7D). The mCherry-Dram1 pattern confirms the predicted membrane localization of Dram1, and Dram1-positive vacuoles were frequently highly decorated by GFP-Lc3 (Figures 7D and S7A). As observed for human macrophages infected with *Mtb* (Figure 4E), zebrafish mCherry-Dram1 colocalizes with and accumulates around *Mm* (Figure 7E). Furthermore, mCherry-Dram1 colocalized with p62 antibody staining during the autophagic response to mycobacterial infection (Figure 7F).

With EM, we determined the ultrastructural composition of *Mm*-containing compartments and regularly observed *Mm* inside autophagolysosomes, as characterized by the presence of cytoplasmic material inside the single-membraned vesicles (Figure S7B). Importantly, we also captured the exact moment at which a double-membraned autophagosome fuses with an *Mm*-containing, electron-dense compartment with the characteristics of a lysosome (Figure 7G). Notably, this event was imaged in a Dram1-overexpressing embryo, and we frequently observed large *Mm*-containing compartments in this treatment group (Figures S7C and S7D). Vesicle fusion would facilitate the delivery of neo-antimicrobial peptides to the bacteria-containing compartment, in line with findings by Ponpuak et al. (2010). The remnants of many membranes inside these compartments demonstrate that these vacuoles have grown to their unusual large size by multiple fusion events.

DISCUSSION

Besides the fundamental cellular homeostatic function of autophagy, selective autophagy has emerged as an important effector mechanism of immune defense (Deretic et al., 2013). Until now, the autophagy modulator DRAM1 was exclusively known as a p53-target gene that induces autophagy and cell death in response to cellular stresses related to cancer (Crighton et al., 2006) and HIV infection of $CD4^+$ T cells (Laforge et al., 2013). Here, we show how this important modulator of autophagy also functions downstream of the TLR/IL1R-MYD88-NF-κB pathway in controlling infection with intracellular mycobacteria independently of p53.

We show that zebrafish Dram1 is capable of modulating autophagy, like its human ortholog (Crighton et al., 2006; Mah et al., 2012), and that *DRAM1* expression is increased in response to infection with mycobacterial pathogens in human macrophages as well as zebrafish embryos. DRAM1/Dram1 colocalizes with mycobacteria and is important for defense against mycobacterial infection. To further support a function of DRAM1 in TB disease progression, we examined published microarray data sets of human patient material for *DRAM1* expression levels and found that *DRAM1* was upregulated in the whole-blood transcript signature of active TB patients (Berry et al., 2010) and in macrophages obtained from *Mtb*-infected patients (Thuong et al., 2008).

Macrophages in *dram1*-deficient zebrafish embryos had difficulty maintaining mycobacteria inside vesicles and were frequently overgrown by bacteria, resulting in large accumulations of extracellular bacteria at later stages of infection. Dram1 and p62 were required for the formation of autophagosomes associated with mycobacterial infection foci. Based on our results, we believe that Dram1 controls intracellular mycobacterial growth in two ways (Figure 7H). First, Dram1 mediates p62-dependent selective autophagy that can engulf entire mycobacteria. Second, Dram1 aids in the maturation of mycobacteria-containing compartments by facilitating multiple fusion

Figure 5. Dram1 Is Required to Contain *Mm* Growth inside Macrophages

(A) Zebrafish embryos injected with standard control morpholino, morpholino against *dram1* (*dram1* Mo 1 and Mo 2), *sqstm1* (*sqstm1* Mo), or *sting* (*sting* Mo) were injected with mCherry-labeled *Mm* (see also Figure S5). Bacterial pixel counts were determined at 4 dpi. Data (mean ± SEM) is pooled from at least two individual experiments (n = 48–76 embryos per group).

(B) Stereo micrographs of the tail region of highly infected standard control, *dram1* Mo 1-, *sqstm1* Mo-, or *sting* Mo-injected embryos. Arrowheads indicate granuloma formation, and arrows indicate accumulation of bacteria in intersegmental veins.

(C) Total numbers of neutrophils and macrophages in 2 dpf control- or *dram1* Mo 1-injected embryos were quantified using a fluorescence stereo microscope (n = 20 per condition, blinded). Total numbers of macrophages were determined by performing whole-mount L-plastin immunohistochemistry and deducting the number of cells positive for neutrophil-specific myeloperoxidase activity from the number of L-plastin-positive total leukocytes per embryo. Each data point represents an individual embryo, and lines indicate the mean.

(D) Expression levels of *il1b* and *mmp9* at 4 dpi in control morpholino-injected and *dram1* Mo 1-injected embryos with or without *Mm* infection (200 colony-forming units [cfu] for control and 50 cfu for *dram1* Mo 1 to obtain equal bacterial burdens) were determined by qPCR (mean ± SEM from n = 3 biological replicates with 20 embryos per pool).

(E and F) Representative confocal micrographs of *mpeg1*:mCherry transgenic embryos injected with control or *dram1* morpholino 1 and infected with GFP-labeled *Mm* or ΔRD1 *Mm* (E) 2 dpi or (F) 3 dpi. Boxed areas are detailed below, with the green and red channels shown separately. Arrowheads indicate bacteria enclosed by membranes.

(G–I) Transmission electron micrograph of control morpholino-injected embryos with bacteria inside a phagosome (G) or bacteria in the cytoplasm (H) or *dram1* morpholino-injected embryos with bacteria present both in phagosomes and in the cytoplasm (I). Arrows indicate cytoplasmic bacteria, while arrowheads indicate phagosomal membranes. Boxed areas are enlarged in the insets, and the dashed line in (I) indicates the remnants of a dead infected cell. See also Figure S5.

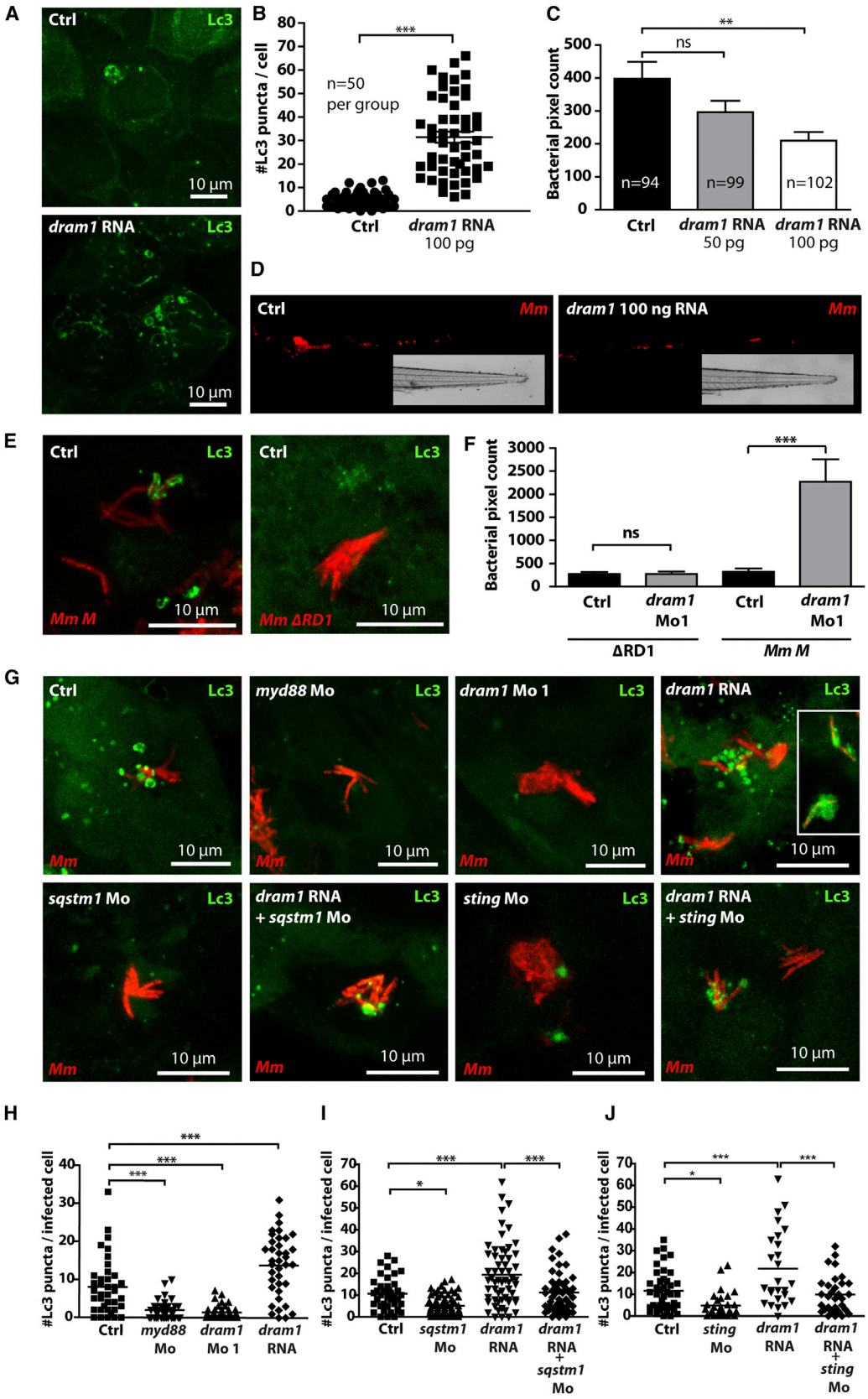

(legend on next page)

events with lysosomes and autophagosomes. It has been shown previously that ribosomal and cytoplasmic peptides taken up via p62-dependent autophagy are proteolytically converted into products capable of killing *Mtb* inside lysosomes (Ponpuak et al., 2010). The stimulation of autophagosomal and lysosomal vesicle fusion by Dram1 can enhance the delivery of such neo-antimicrobial peptides. In the absence of *dram1*, GFP-Lc3 accumulation could still be induced by Ar-12 or rapamycin, indicating that these drugs stimulate nonselective autophagy pathways independent of Dram1. Ar-12 and rapamycin enhance bacterial killing in several model systems (Chiu et al., 2009a, 2009b; Romagnoli et al., 2012). However, contrary to the protective effect of *dram1* overexpression, Ar-12 or rapamycin treatments were detrimental to defense in the zebrafish model, most likely due to susceptibility of zebrafish embryos to broad side effects of these drugs.

The targeting of autophagosomes to mycobacteria by Dram1 required the DNA-sensing Sting pathway. In human macrophages, the STING pathway was shown to ubiquitinate and target *Mtb* for autophagic destruction after bacteria had permeabilized the phagosomal membrane using a RD1 locus encoded virulence mechanism (Watson et al., 2012). In contrast, RD1 virulence was linked with inhibition of autophagy in *Mtb*-infected dendritic cells (Romagnoli et al., 2012). While autophagy-evading strategies are likely to have evolved in mycobacteria, our results in the zebrafish model corroborate the essential requirement of RD1 and Sting for selective autophagic defense against mycobacteria (Lerena and Colombo, 2011; Watson et al., 2012).

TLR/IL1R signaling via the MYD88-dependent and -independent pathways can activate tumor necrosis factor receptor-associated factor (TRAF)-associated NF-κB activator (TANK)-binding kinase-1 (TBK1) (Clark et al., 2011), which coordinates assembly and function of the autophagic machinery, including phosphorylation of p62 and maturation of autophagosomes (Pilli et al., 2012). The IKK family member TBK1 can activate NF-κB (Pomerantz and Baltimore, 1999), making it a potential regulator of *DRAM1* and infection-induced autophagy. However, TBK1 can also inhibit the canonical IKK complex (Clark et al., 2011), known to be involved in initiation of autophagy (Criollo et al., 2010). It is becoming clear that autophagy is regulated by both the canonical and noncanonical NF-κB activation pathways, as well as the stress-induced p53 pathway (Criollo et al., 2010). Besides NF-κB-binding motifs, we identified consensus binding sites for AP-1 and STAT in the promoter region of DRAM1, indicating that other immune signaling pathways may also activate DRAM1. Further dissection of DRAM1 regulation will help clarify the complex signaling networks controlling autophagy initiation and flux in response to different stimuli.

The diverse roles of autophagy as both effector and regulator of immune processes are receiving much attention (Deretic et al., 2013). Here, we showed that the TLR/IL1R-MYD88-NF-κB-dependent expression of *dram1* is required to mobilize autophagic defense to mycobacteria. Zebrafish *dram1* expression is also upregulated by *Salmonella* infection (Stockhammer et al., 2010), and in the current study we showed it to be responsive to the common bacterial endotoxin LPS. Furthermore, autophagic defense against intestinal bacteria was recently shown to depend on MYD88, but how MYD88 is linked with autophagosome induction remained unknown (Benjamin et al., 2013). In light of these observations, we expect this TLR-MYD88-DRAM1 defense pathway to protect against a range of intracellular pathogens broader than that of mycobacterial species alone. The role of DRAM1 in immunity might even be broader than that. First, autophagy functions as a regulator of inflammation by targeting inflammasomes for degradation, limiting the processing and secretion of IL-1β (Shi et al., 2012). Knockdown of zebrafish *dram1* increased *il1b* expression levels following mycobacterial infection, linking DRAM1 to the regulatory immune function of autophagy. Second, particles that stimulate TLRs during phagocytosis trigger the rapid recruitment of LC3 to the phagosome in a process termed LC3-associated phagocytosis (LAP) (Sanjuan et al., 2007). With the currently available techniques, we could not ascertain if Dram1 is involved in LAP; however, *dram1* depletion led to a notable absence of autophagolysosomes, consistent with the proposed role in autophagosome maturation (Figure 7H).

The increasing occurrence of *Mtb* strains with resistance to multiple drug treatments makes TB a key priority for infectious disease research. Understanding the host-pathogen interactions during *Mtb* pathogenesis is necessary to develop host-directed therapeutic strategies that may complement antibiotic interventions (Koul et al., 2011; Kuijl et al., 2007). The role of DRAM1 as an inducer of antimycobacterial autophagy makes this pathway a highly interesting therapeutic target, since we have shown in vivo that hyperactivation of the DRAM1-dependent autophagy pathway significantly lowered mycobacterial burden.

Figure 6. Dram1 Modulates an Autophagic Defense Mechanism that Requires Bacterial RD1 Virulence, Host p62/Sqstm1, and Sting

(A) GFP-Lc3 embryos were injected with 100 pg *dram1* RNA. Representative confocal micrographs of epithelial cells at 3 dpf are shown.

(B) The number of GFP-Lc3 punctae was determined for n = 50 cells per group and quantified based on confocal micrographs of control- and *dram1* RNA-injected embryos ($n \geq 5$, blinded).

(C) Bacterial pixel counts were determined at 3 dpi for infected control- or *dram1* RNA-injected embryos. Data (mean ± SEM) is pooled from two individual experiments ($n \geq 94$ embryos per group).

(D) Representative stereo micrographs of the tail of infected control- or *dram1* RNA-injected embryos at 3 dpi.

(E) Representative confocal micrographs of GFP-Lc3 embryos infected with *Mm M* ΔRD1 (400 cfu) and wild-type *Mm M* bacteria (200 cfu).

(F) Bacterial pixel counts following these infections were determined with or without *dram1* knockdown. Data (mean ± SEM) are pooled from two individual experiments ($n > 62$ embryos per group).

(G) Representative confocal micrographs of GFP-Lc3 embryos injected with control morpholino, *myd88* morpholino, *dram1* morpholino 1, *dram1* RNA (100 pg; inset in the image is a micrograph from a different RNA-injected embryo), *sqstm1* morpholino, *dram1* RNA + *sqstm1* morpholino, *sting* morpholino, and *dram1* RNA + *sting* morpholino. All groups were injected with *Mm*.

(H–J) Confocal micrographs were used to quantify GFP-Lc3 punctae per infected cell ($n \geq 5$ embryos per group, blinded) to evaluate the effect of *dram1* RNA (H), *dram1* RNA combined with *sqstm1* Mo (I), or *dram1* RNA combined with *sting* Mo (J). See also Figure S6.

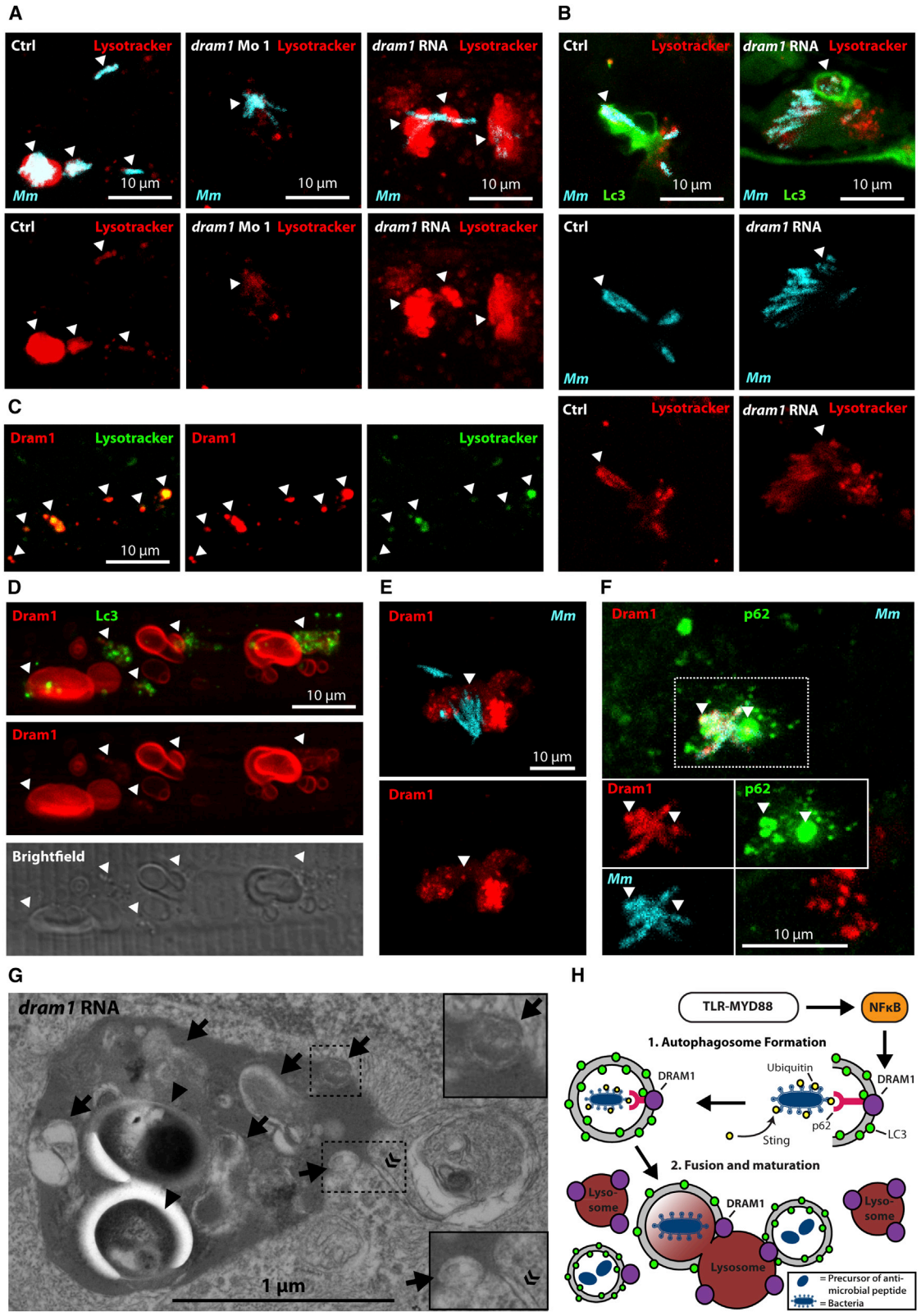

Figure 7. Dram1 Mediates Autophagic Flux and Lysosomal Maturation via Multiple Vesicle Fusion Events

(A and B) Embryos were infected with crimson-labeled *Mm* and stained with LysoTracker Red (arrowheads indicate colocalization). (A) Wild-type embryos injected with standard control, *dram1* morpholino, or *dram1* RNA (100 pg). (B) *dram1* RNA- or control-injected GFP-Lc3 embryos.

(legend continued on next page)

EXPERIMENTAL PROCEDURES

Zebrafish Culture and Lines

Zebrafish lines (Table S1) were handled in compliance with local animal welfare regulations as overseen by the Leiden University animal ethics committee. Embryos were grown at 28.5°C and kept under anesthesia with egg water containing 0.02% buffered 3-aminobenzoic acid ethyl ester (Tricaine) during bacterial injections or imaging.

Injection Conditions

Mycobacteria or LPS was injected into zebrafish embryos as described in the Supplemental Experimental Procedures. Splice morpholinos (Table S2) and RNA were injected into the yolk, and mCherry-Dram1 was injected into the cell, at the one-cell stage (details in Supplemental Experimental Procedures). Morpholino knockdown of mRNA was tested using the SuperScript One-Step RT-PCR System (Invitrogen, #10928-034).

Gene Expression Analysis

RNA was isolated using TRI Reagent (Life Technologies) and purified with RNeasy MinElute Cleanup kit (QIAGEN). cDNA synthesis and qPCR (Table S3 for primer sequences) were performed as described previously (van der Vaart et al., 2013), and gene expression was normalized against housekeeping genes. Microarray and RNA sequencing analysis was performed as described in the Supplemental Experimental Procedures. Macrophages, neutrophils, and lymphocytes were isolated by FACS from 5–6 dpf zebrafish larvae.

Drug Treatments

The following drugs were used: 3-methyladenine (3-MA; 10 mM; Sigma, #M9281), chloroquine (100 μM; Sigma, #C6628), Ar-12 (1 μM; Selleck Chemicals, #S1106), Rapamycin (1 μM; Sigma, #44532-U), NF-κB activation inhibitor (50 nM in embryos, 30 nM in macrophages; Calbiochem, #481406), and Roscovitin (50 μM; Sigma, #R7772). Drugs were administered via the water or culture medium for zebrafish embryos and human macrophages, respectively.

Microscopy and Fluorescent Pixel Quantification

Embryos were imaged using a Leica MZ16FA stereo fluorescence microscope with DFC420C camera or a Leica TCS SPE confocal microscope. Maximal intensity projections of confocal micrograph z stacks are shown. Total fluorescent pixels per infected fish were determined on whole-embryo stereo fluorescent micrographs using dedicated software (Cui et al., 2011). Electron microscopy images were obtained with a JEOL JEM-1010 transmission electron microscope equipped with an Olympus MegaView camera (see Supplemental Experimental Procedures for sample preparation).

Immunohistochemistry

Identification of neutrophils and macrophages was done by immunolabeling with a leukocyte-specific L-plastin antibody and Alexa 568 conjugated secondary antibody combined with neutrophil-specific staining for myeloperoxidase activity (Cui et al., 2011). p62 was detected by a sheep polyclonal antibody (ab31545, Abcam); human DRAM1 (AP21751PU-N, Acris Antibodies) and LC3 (PA1-46286, Thermo Scientific) were detected by rabbit polyclonal antibodies combined with donkey-anti-sheep/goat-anti-rabbit Alexa488 conjugated secondary antibody (Invitrogen).

LysoTracker Staining

Embryos were incubated for 1 hr in egg water with 10 μM LysoTracker Green or Red (Invitrogen) and rinsed several times before imaging.

Infection of Human Macrophages

Type 1 and 2 human macrophages were generated from buffy coats of anonymous blood bank donors with approval of the medical ethical committee of the Leiden University Medical Center, and they were maintained and transfected with siRNA as described in detail in the Supplemental Experimental Procedures. *Mtb* was cultured in Difco Middlebrook 7H9 broth (Becton Dickinson) supplemented with 10% albumin dextrose catalase (ADC) (Becton Dickinson) and 0.5% Tween-80 (Sigma). Primary human macrophages were infected at a multiplicity of infection (moi) of 10. Wells containing the cell cultures were inoculated with 100 μl of *Mtb* suspension, centrifuged for 3 min at 800 rpm, and incubated at 37°C/5% CO_2 for 60 min. Plates were then washed with medium containing 30 mg/ml gentamicin sulfate (Lonza BioWhittaker) and incubated at 37°C/5% CO_2 in medium containing 5 mg/ml gentamicin and inhibitors, if appropriate.

Statistical Analysis

All data (mean ± SEM) were analyzed using unpaired, two-tailed t tests for comparisons between two groups and one-way ANOVA with Tukey's multiple comparison method as a posthoc test for other data. (ns, no significant difference; *$p < 0.05$; **$p < 0.01$; ***$p < 0.001$). For microarray, significant differences were calculated using Rosetta Resolver re-ratio analysis (* = fold change > 2, $p < 10^{-5}$). For RNA deep sequencing, significant differences were calculated by DESeq analysis of transcript count data (* = fold change > 2, $p < 0.05$).

ACCESSION NUMBERS

Microarray and RNA sequencing data were deposited in the Gene Expression Omnibus (GEO) database under accession number GSE49188.

SUPPLEMENTAL INFORMATION

Supplemental Information includes Supplemental Experimental Procedures, seven figures, and three tables and can be found with this article online at http://dx.doi.org/10.1016/j.chom.2014.05.005.

ACKNOWLEDGMENTS

We thank Phil Elks and Serge Mostowy for helpful discussions; Alex Nezhinsky and Fons Verbeek for pixel quantification software; Kimberley Walburg, Rubén Marín-Juez, Vincenzo Torraca, Zakia Kanwal, Erica Benard, and Julien Rougeot for valuable contributions; and Ulrike Nehrdich and Davy de Witt for fish care. This work was supported by the Smart Mix Program of the Netherlands Ministry of Economic Affairs and the Ministry of Education, Culture and Science and the European projects ZF-HEALTH (HEALTH-F4-2010-242048), FishForPharma (PITN-GA-2011-289209), PHAGOSYS (HEALTH-F4-2008-223451), NEWTBVAC, and ADITEC (grant agreement 280873), and the Netherlands Relief Foundation.

Received: August 15, 2013
Revised: January 28, 2014
Accepted: April 24, 2014
Published: June 11, 2014

REFERENCES

Alonso, S., Pethe, K., Russell, D.G., and Purdy, G.E. (2007). Lysosomal killing of Mycobacterium mediated by ubiquitin-derived peptides is enhanced by autophagy. Proc. Natl. Acad. Sci. USA *104*, 6031–6036.

Benjamin, J.L., Sumpter, R., Jr., Levine, B., and Hooper, L.V. (2013). Intestinal epithelial autophagy is essential for host defense against invasive bacteria. Cell Host Microbe *13*, 723–734.

Berg, R.D., and Ramakrishnan, L. (2012). Insights into tuberculosis from the zebrafish model. Trends Mol. Med. *18*, 689–690.

(C–F) Embryos transiently expressing mCherry-Dram1, colocalized with (C) LysoTracker Green, (D) GFP-Lc3, (E) crimson-labeled *Mm*, or (F) crimson-labeled *Mm*, and immunohistochemistry detection of p62 (arrowheads indicate colocalization).
(G) Transmission electron micrograph of *dram1* RNA-injected embryos infected with *Mm* (arrowheads). Arrows indicate (remnants of) vesicle fusion, and « indicates the double membrane of an autophagosome.
(H) Schematic representation of the findings presented in this manuscript, as explained in the Discussion. See also Figure S7.

Bernut, A., Herrmann, J.L., Kissa, K., Dubremetz, J.F., Gaillard, J.L., Lutfalla, G., and Kremer, L. (2014). Mycobacterium abscessus cording prevents phagocytosis and promotes abscess formation. Proc. Natl. Acad. Sci. USA *111*, E943–E952.

Berry, M.P., Graham, C.M., McNab, F.W., Xu, Z., Bloch, S.A., Oni, T., Wilkinson, K.A., Banchereau, R., Skinner, J., Wilkinson, R.J., et al. (2010). An interferon-inducible neutrophil-driven blood transcriptional signature in human tuberculosis. Nature *466*, 973–977.

Chiu, H.C., Kulp, S.K., Soni, S., Wang, D., Gunn, J.S., Schlesinger, L.S., and Chen, C.S. (2009a). Eradication of intracellular Salmonella enterica serovar Typhimurium with a small-molecule, host cell-directed agent. Antimicrob. Agents Chemother. *53*, 5236–5244.

Chiu, H.C., Soni, S., Kulp, S.K., Curry, H., Wang, D., Gunn, J.S., Schlesinger, L.S., and Chen, C.S. (2009b). Eradication of intracellular Francisella tularensis in THP-1 human macrophages with a novel autophagy inducing agent. J. Biomed. Sci. *16*, 110.

Clark, K., Peggie, M., Plater, L., Sorcek, R.J., Young, E.R., Madwed, J.B., Hough, J., McIver, E.G., and Cohen, P. (2011). Novel cross-talk within the IKK family controls innate immunity. Biochem. J. *434*, 93–104.

Clay, H., Davis, J.M., Beery, D., Huttenlocher, A., Lyons, S.E., and Ramakrishnan, L. (2007). Dichotomous role of the macrophage in early Mycobacterium marinum infection of the zebrafish. Cell Host Microbe *2*, 29–39.

Crighton, D., Wilkinson, S., O'Prey, J., Syed, N., Smith, P., Harrison, P.R., Gasco, M., Garrone, O., Crook, T., and Ryan, K.M. (2006). DRAM, a p53-induced modulator of autophagy, is critical for apoptosis. Cell *126*, 121–134.

Criollo, A., Senovilla, L., Authier, H., Maiuri, M.C., Morselli, E., Vitale, I., Kepp, O., Tasdemir, E., Galluzzi, L., Shen, S., et al. (2010). IKK connects autophagy to major stress pathways. Autophagy *6*, 189–191.

Cui, C., Benard, E.L., Kanwal, Z., Stockhammer, O.W., van der Vaart, M., Zakrzewska, A., Spaink, H.P., and Meijer, A.H. (2011). Infectious disease modeling and innate immune function in zebrafish embryos. Methods Cell Biol. *105*, 273–308.

Delgado, M.A., Elmaoued, R.A., Davis, A.S., Kyei, G., and Deretic, V. (2008). Toll-like receptors control autophagy. EMBO J. *27*, 1110–1121.

Deretic, V., Saitoh, T., and Akira, S. (2013). Autophagy in infection, inflammation and immunity. Nat. Rev. Immunol. *13*, 722–737.

Ellett, F., Pase, L., Hayman, J.W., Andrianopoulos, A., and Lieschke, G.J. (2011). mpeg1 promoter transgenes direct macrophage-lineage expression in zebrafish. Blood *117*, e49–e56.

Galavotti, S., Bartesaghi, S., Faccenda, D., Shaked-Rabi, M., Sanzone, S., McEvoy, A., Dinsdale, D., Condorelli, F., Brandner, S., Campanella, M., et al. (2013). The autophagy-associated factors DRAM1 and p62 regulate cell migration and invasion in glioblastoma stem cells. Oncogene *32*, 699–712.

Gao, M., Yeh, P.Y., Lu, Y.S., Hsu, C.H., Chen, K.F., Lee, W.C., Feng, W.C., Chen, C.S., Kuo, M.L., and Cheng, A.L. (2008). OSU-03012, a novel celecoxib derivative, induces reactive oxygen species-related autophagy in hepatocellular carcinoma. Cancer Res. *68*, 9348–9357.

Guo, L., Liew, H.P., Camus, S., Goh, A.M., Chee, L.L., Lunny, D.P., Lane, E.B., and Lane, D.P. (2013). Ionizing radiation induces a dramatic persistence of p53 protein accumulation and DNA damage signaling in mutant p53 zebrafish. Oncogene *32*, 4009–4016.

Gutierrez, M.G., Master, S.S., Singh, S.B., Taylor, G.A., Colombo, M.I., and Deretic, V. (2004). Autophagy is a defense mechanism inhibiting BCG and Mycobacterium tuberculosis survival in infected macrophages. Cell *119*, 753–766.

He, C., Bartholomew, C.R., Zhou, W., and Klionsky, D.J. (2009). Assaying autophagic activity in transgenic GFP-Lc3 and GFP-Gabarap zebrafish embryos. Autophagy *5*, 520–526.

Kanther, M., Sun, X., Mühlbauer, M., Mackey, L.C., Flynn, E.J., 3rd, Bagnat, M., Jobin, C., and Rawls, J.F. (2011). Microbial colonization induces dynamic temporal and spatial patterns of NF-κB activation in the zebrafish digestive tract. Gastroenterology *141*, 197–207.

Koul, A., Arnoult, E., Lounis, N., Guillemont, J., and Andries, K. (2011). The challenge of new drug discovery for tuberculosis. Nature *469*, 483–490.

Kuijl, C., Savage, N.D., Marsman, M., Tuin, A.W., Janssen, L., Egan, D.A., Ketema, M., van den Nieuwendijk, R., van den Eeden, S.J., Geluk, A., et al. (2007). Intracellular bacterial growth is controlled by a kinase network around PKB/AKT1. Nature *450*, 725–730.

Laforge, M., Limou, S., Harper, F., Casartelli, N., Rodrigues, V., Silvestre, R., Haloui, H., Zagury, J.F., Senik, A., and Estaquier, J. (2013). DRAM triggers lysosomal membrane permeabilization and cell death in CD4(+) T cells infected with HIV. PLoS Pathog. *9*, e1003328.

Langenau, D.M., Ferrando, A.A., Traver, D., Kutok, J.L., Hezel, J.P., Kanki, J.P., Zon, L.I., Look, A.T., and Trede, N.S. (2004). In vivo tracking of T cell development, ablation, and engraftment in transgenic zebrafish. Proc. Natl. Acad. Sci. USA *101*, 7369–7374.

Lerena, M.C., and Colombo, M.I. (2011). Mycobacterium marinum induces a marked LC3 recruitment to its containing phagosome that depends on a functional ESX-1 secretion system. Cell. Microbiol. *13*, 814–835.

Levine, B., Mizushima, N., and Virgin, H.W. (2011). Autophagy in immunity and inflammation. Nature *469*, 323–335.

Mah, L.Y., O'Prey, J., Baudot, A.D., Hoekstra, A., and Ryan, K.M. (2012). DRAM-1 encodes multiple isoforms that regulate autophagy. Autophagy *8*, 18–28.

Mostowy, S., Boucontet, L., Mazon Moya, M.J., Sirianni, A., Boudinot, P., Hollinshead, M., Cossart, P., Herbomel, P., Levraud, J.P., and Colucci-Guyon, E. (2013). The zebrafish as a new model for the in vivo study of Shigella flexneri interaction with phagocytes and bacterial autophagy. PLoS Pathog. *9*, e1003588.

Pilli, M., Arko-Mensah, J., Ponpuak, M., Roberts, E., Master, S., Mandell, M.A., Dupont, N., Ornatowski, W., Jiang, S., Bradfute, S.B., et al. (2012). TBK-1 promotes autophagy-mediated antimicrobial defense by controlling autophagosome maturation. Immunity *37*, 223–234.

Pomerantz, J.L., and Baltimore, D. (1999). NF-kappaB activation by a signaling complex containing TRAF2, TANK and TBK1, a novel IKK-related kinase. EMBO J. *18*, 6694–6704.

Ponpuak, M., Davis, A.S., Roberts, E.A., Delgado, M.A., Dinkins, C., Zhao, Z., Virgin, H.W., 4th, Kyei, G.B., Johansen, T., Vergne, I., and Deretic, V. (2010). Delivery of cytosolic components by autophagic adaptor protein p62 endows autophagosomes with unique antimicrobial properties. Immunity *32*, 329–341.

Ramakrishnan, L. (2012). Revisiting the role of the granuloma in tuberculosis. Nat. Rev. Immunol. *12*, 352–366.

Renshaw, S.A., Loynes, C.A., Trushell, D.M., Elworthy, S., Ingham, P.W., and Whyte, M.K. (2006). A transgenic zebrafish model of neutrophilic inflammation. Blood *108*, 3976–3978.

Romagnoli, A., Etna, M.P., Giacomini, E., Pardini, M., Remoli, M.E., Corazzari, M., Falasca, L., Goletti, D., Gafa, V., Simeone, R., et al. (2012). ESX-1 dependent impairment of autophagic flux by Mycobacterium tuberculosis in human dendritic cells. Autophagy *8*, 1357–1370.

Ryan, K.M. (2011). p53 and autophagy in cancer: guardian of the genome meets guardian of the proteome. Eur. J. Cancer *47*, 44–50.

Sanjuan, M.A., Dillon, C.P., Tait, S.W.G., Moshiach, S., Dorsey, F., Connell, S., Komatsu, M., Tanaka, K., Cleveland, J.L., Withoff, S., and Green, D.R. (2007). Toll-like receptor signalling in macrophages links the autophagy pathway to phagocytosis. Nature *450*, 1253–1257.

Shi, C.S., and Kehrl, J.H. (2008). MyD88 and Trif target Beclin 1 to trigger autophagy in macrophages. J. Biol. Chem. *283*, 33175–33182.

Shi, C.S., Shenderov, K., Huang, N.N., Kabat, J., Abu-Asab, M., Fitzgerald, K.A., Sher, A., and Kehrl, J.H. (2012). Activation of autophagy by inflammatory signals limits IL-1β production by targeting ubiquitinated inflammasomes for destruction. Nat. Immunol. *13*, 255–263.

Singh, S.B., Davis, A.S., Taylor, G.A., and Deretic, V. (2006). Human IRGM induces autophagy to eliminate intracellular mycobacteria. Science *313*, 1438–1441.

Stockhammer, O.W., Rauwerda, H., Wittink, F.R., Breit, T.M., Meijer, A.H., and Spaink, H.P. (2010). Transcriptome analysis of Traf6 function in the innate immune response of zebrafish embryos. Mol. Immunol. *48*, 179–190.

Swaim, L.E., Connolly, L.E., Volkman, H.E., Humbert, O., Born, D.E., and Ramakrishnan, L. (2006). Mycobacterium marinum infection of adult zebrafish causes caseating granulomatous tuberculosis and is moderated by adaptive immunity. Infect. Immun. *74*, 6108–6117.

Thuong, N.T., Dunstan, S.J., Chau, T.T., Thorsson, V., Simmons, C.P., Quyen, N.T., Thwaites, G.E., Thi Ngoc Lan, N., Hibberd, M., Teo, Y.Y., et al. (2008). Identification of tuberculosis susceptibility genes with human macrophage gene expression profiles. PLoS Pathog. *4*, e1000229.

van der Vaart, M., van Soest, J.J., Spaink, H.P., and Meijer, A.H. (2013). Functional analysis of a zebrafish myd88 mutant identifies key transcriptional components of the innate immune system. Dis. Model. Mech. *6*, 841–854.

van der Wel, N., Hava, D., Houben, D., Fluitsma, D., van Zon, M., Pierson, J., Brenner, M., and Peters, P.J. (2007). M. tuberculosis and M. leprae translocate from the phagolysosome to the cytosol in myeloid cells. Cell *129*, 1287–1298.

Vergne, I., Chua, J., Singh, S.B., and Deretic, V. (2004). Cell biology of mycobacterium tuberculosis phagosome. Annu. Rev. Cell Dev. Biol. *20*, 367–394.

Watson, R.O., Manzanillo, P.S., and Cox, J.S. (2012). Extracellular M. tuberculosis DNA targets bacteria for autophagy by activating the host DNA-sensing pathway. Cell *150*, 803–815.

Zhang, X.D., Qi, L., Wu, J.C., and Qin, Z.H. (2013). DRAM1 regulates autophagy flux through lysosomes. PLoS ONE *8*, e63245.